Geosci. Model Dev. Discuss., doi:10.5194/gmd-2017-61, 2017
Manuscript under review for journal Geosci. Model Dev.
Discussion started: 15 March 2017

Geoscientific Model Development Discussions
Open Access
EGU

A new urban surface model integrated in the large-eddy simulation model PALM

Jaroslav Resler[1, 2], Pavel Krč[1, 2], Michal Belda[1, 2, 4], Pavel Juruš[1, 2], Nina Benešová[1, 3], Jan Lopata[1, 3], Ondřej Vlček[1, 3], Daša Damašková[1, 3], Kryštof Eben[1, 2], Přemysl Derbek[1], Björn Maronga[5], and Farah Kanani-Sühring[5]

[1]Faculty of Transportation Sciences, Czech Technical University in Prague, Czech Republic
[2]Institute of Computer Science, The Czech Academy of Sciences, Prague, Czech Republic
[3]Air Quality Protection Division, Czech Hydrometeorological Institute, Prague, Czech Republic
[4]Department of Atmospheric Physics, Faculty of Mathematics and Physics, Charles University, Prague, Czech Republic
[5]Institute of Meteorology and Climatology, Leibniz Universität Hannover, Hannover, Germany

Correspondence to: Jaroslav Resler (reslejar@fd.cvut.cz)

Abstract. Urban areas are an important part of the climate system and many aspects of urban climate have a direct effect on human health and living conditions. This implies the need for a reliable tool for climatology studies that supports urban planning and development strategies. However, a realistic implementation of urban canopy processes still poses a serious challenge for weather and climate modelling for the current generation of numerical models. To address this demand, a new model of energy processes for urban environments was developed as an Urban Surface Model (USM) and integrated as a module into the large-eddy simulation (LES) model PALM. The USM contains a multi-reflection radiation model for short and long wave radiation, calculation of the energy balance on horizontal and vertical impervious surfaces, thermal diffusion in ground, wall and roof materials and anthropogenic heat from transportation. The module also models absorption of radiation by resolved plant canopy (i.e. trees, shrubs). The USM was parallelized using MPI and performance testing demonstrates that the computational costs of the USM are reasonable and the model scales well on typical cluster configurations. The module was fully integrated into PALM and is available via its online repository under GNU General Public License (GPL). The implementation was tested on a summer heat wave episode in the real conditions of a selected Prague crossroad. General patterns of temperature of various surface types (walls, pavement) are in good agreement with observations. The coupled LES-USM system appears to correct the bias found between observations and mesoscale model predictions for the near-surface air temperature. The results, however, show a strong dependence on the prescribed surface and wall material properties. Their exact knowledge is thus essential for the correct prediction of the flow in the urban canopy layer.

1 Introduction

1.1 Urban climate

Urban areas constitute an important part of the climate system. As more than a half of the human population resides in cities, and this figure is expected to keep increasing (United Nations 2014), the influence of urban surfaces on the climate gains more

Geosci. Model Dev. Discuss., doi:10.5194/gmd-2017-61, 2017
Manuscript under review for journal Geosci. Model Dev.
Discussion started: 15 March 2017

Geoscientific Model Development Discussions
Open Access
EGU

importance. Many aspects of urban climate have a direct effect on human health and living conditions, the most prominent examples being thermal comfort and air quality. These effects can be further amplified in the changing climate. Thus, a need arises on the side of decision makers for a sound scientific background for adaptation and mitigation strategies.

One of the major phenomena of the urban climate is the urban heat island, i.e. the fact that an urban area may be significantly warmer than its surrounding rural areas (Oke, 1995). The increase of temperature is linked to the difference in absorption and retention of energy by urban surfaces, which can cause a difference in the order of several degrees Celsius. On the opposite side is the urban cool island, the effect of decreased temperatures due to the shadowing of the surfaces by buildings. Several possible approaches to studying urban climate have been used ranging from observation analyses, physical modelling to numerical simulations (for a comprehensive review see e.g. Mirzaei and Haghighat, 2010; Moonen et al., 2012).

Modelling of the urban climate is a topic which encompasses a number of physical processes and their complex interactions (e.g. Arnfield, 2003). Urban surfaces are affected by shortwave and longwave radiation, and energy is exchanged between various components of urban canopy and atmosphere in various forms – including sensible and latent heat fluxes. These fluxes, together with boundary-layer processes and large-scale synoptic conditions, in turn, affect the turbulent flow of air. The complexity is further increased by the presence of vegetation and high heterogeneity of urban surface materials. All these parameters together affect human thermal comfort.

Various approaches and frameworks have been used for numerical modelling of urban climate processes; their comprehensive summarisation can be found in reviews by Mirzaei and Haghighat (2010), Moonen et al. (2012) or Mirzaei (2015). A common approach is to use a parameterization of the urban canopy layer within a regional meteorological or climate model (e.g. WRF, Skamarock et al., 2008). One of the main difficulties with this approach, however, is reaching sufficiently high resolution. A typical mesoscale numerical weather prediction or regional climate model operates with horizontal resolution in the order of hundreds of metres to tens of kilometres. However, components comprising cities are constructed on much smaller scales. Dimensions of a typical street canyon are two or three orders of magnitude finer and thus inherently invisible to these models.

A second approach is represented by standalone parameterized models, e.g. the SOLWEIG model (Lindberg et al., 2008), RayMan (Matzarakis et al., 2010), TUF-3D model (Krayenhoff and Voogt, 2007), TEB (Masson, 2000) or SUEWS (Järvi et al., 2011). These models treat some physical processes (e.g. radiation, latent heat flux, water balance) while they parameterize interaction with air flow by means of statistical and climatological models or meteorological measurements.

The most complex approach is represented by a group of computational fluid dynamics (CFD) models. The modelling of the turbulent flow is computationally expensive, thus, different techniques are used to make calculations feasible, usually based on limiting the resolved range of the length and time scales. Most of the CFD models used for urban climatology studies today are models using Reynolds-Averaged Navier-Stokes equations (RANS) technique e.g. ENVI-met (ENVI-met, 2009), MITRAS (Schlünzen et al., 2003), MIMO (Ehrhard et al., 2000) and MUKLIMO_3 (Sievers, 2012, 2014). In RANS models, the entire turbulence spectrum is parameterized, and thus only the mean flow can be predicted. This allows for using relatively large time steps leading to moderate computational demands, but it implies physical limitations as interactions of turbulent eddies with the urban canopy cannot be explicitly treated. In order to overcome this deficiency, Large-Eddy Simulation (LES) models can be

Geosci. Model Dev. Discuss., doi:10.5194/gmd-2017-61, 2017
Manuscript under review for journal Geosci. Model Dev.
Discussion started: 15 March 2017

Geoscientific Model Development Discussions

employed. They use a scale separation approach to resolve the bulk of the turbulence spectrum explicitly, while parameterizing only the smallest eddies in a so-called subgrid-scale model. An example of such a model is PALM (Maronga et al., 2015). The modelling system OpenFoam[1] comprises both, LES and RANS solvers. Many of the models do not contain appropriate radiative models. To overcome this deficiency, an independent radiative model can be used, with the resulting radiation fluxes imported into the CFD model (e.g. SOLENE-microclimat, Musy et al., 2015). Most of the mentioned models are closed source in-house solutions which makes their scientific and technical validation difficult. Many of them are also not designed to work on high-performance computing (HPC) systems which limits their applications. By contrast, PALM and OpenFoam models are available under a free license and can be run in parallel on large HPC systems.

One of the tasks in the Urban Adapt project[2], which this work was part of, was the evaluation of urban planning scenarios assessing the influence of urban surface parameters and vegetation on pedestrian-level air quality and thermal comfort for citizens. Regarding these problems, CFD-LES models can be considered to be the most appropriate as they can predict the turbulent air flow with sufficient resolution over a very complex surface. Nevertheless, according to the authors' research at the beginning of the study there was no open source CFD-LES model that would be able to account for the realistic implementation of various processes inside an urban canopy. Therefore, we decided to extend the existing LES model PALM with a submodel that explicitly describes energy exchanges in the urban environment, including some of the most important urban canopy mechanisms.

1.2 The LES model PALM

The LES model PALM (Maronga et al., 2015) is designed to simulate a flow in atmospheric and oceanic boundary layers. A highlight of PALM is its outstanding scalability on massively parallel computer architectures. The model solves the non-hydrostatic incompressible Navier-Stokes equations in Boussinesq approximation. Subgrid-scale processes that cannot be resolved implicitly based on the numerical grid resolution are parameterized according to the 1.5-order Deardorff closure scheme (Deardorff, 1980) with the modification of Moeng and Wyngaard (1988) and Saiki et al. (2000), with the assumption that the energy transport by subgrid-scale eddies is proportional to the local gradients of the mean quantities.

Prognostic equations are solved numerically, primarily using an upwind biased fifth-order differencing scheme (Wicker and Skamarock, 2002) and a third-order Runge-Kutta time stepping scheme after Williamson (1980). Discretization in space is achieved using finite differences on a staggered Cartesian Arakawa-C grid (Arakawa and Lamb, 1977).

PALM includes several schemes representing physical processes, such as cloud microphysics, a plant canopy model and an embedded Lagrangian particle model. In connection to the urban application, four other relevant schemes are already implemented. First, PALM offers a Cartesian topography scheme that covers solid, impermeable, fixed flow obstacles (e.g. hills or buildings). A constant-flux layer is assumed between each surface element and the first grid level adjacent to the respective surface in order to account for friction effects. Next, the representation of radiative exchange is implemented with three options: constant radiation, simple clear-sky radiation parameterization, and coupling with Rapid Radiation Transfer Model for Global

[1] http://www.openfoam.org
[2] http://urbanadapt.cz/en

Geosci. Model Dev. Discuss., doi:10.5194/gmd-2017-61, 2017
Manuscript under review for journal Geosci. Model Dev.
Discussion started: 15 March 2017

Geoscientific Model Development Discussions

Models (RRTMG, e.g. Clough et al., 2005), which is applied as a single column model for each vertical column in the PALM domain. Moreover, PALM has the capability of using large-scale model data (e.g. from mesoscale models such as WRF) as forcing data through tendency terms, including an option for model nudging. Finally, land surface interactions with the atmosphere are implemented based on a simplified version of the Tiled European Centre for Medium-Range Weather Forecasts Scheme for Surface Exchanges over Land (TESSEL/HTESSEL, Balsamo et al., 2009) and its derivative implementation on the DALES model (Heus et al., 2010). The PALM land surface submodel (Maronga and Bosveld, 2017), hereafter referred to as PALM-LSM, includes a parameterization for impervious surfaces on the ground (pavements, roads) by replacing upper soil layers with a pavement layer attributed with a specific heat capacity and heat conductivity and allowing to hold a maximum of 1 mm liquid water from precipitation. However, none of the included schemes are suited for treating complex effects of the urban environment driven by the diverse physical properties of different urban surfaces (both horizontal and vertical), heat transfer within building walls, and heat flux between the urban surfaces and the atmosphere. Also the description of shortwave and longwave radiation budgets including shading and multi-reflection, and absorption of radiation by plant canopies was not treated by PALM so far. Therefore, we developed an urban surface model for PALM that is able to treat these processes using approaches described in the following section.

2 Urban surface model

In this section, a new urban surface model (USM) for PALM is described. The USM consists of a solver for the energy balance of all horizontal and vertical urban surface elements, including building walls and roofs, as well as pavements. The energy balance solver predicts the skin layer temperature and simultaneously calculates the near-surface turbulent flux of sensible heat as well as the heat flux into the material. The latter is calculated by means of a multi-layer material model predicting heat diffusion through solid material. Moreover, a multi-reflection radiative transfer model for the urban canopy layer was implemented, and coupled to the plant canopy model in order to calculate realistic surface radiative fluxes as input for the energy balance solver.

2.1 Energy balance solver

The surface energy balance correlates radiative energy fluxes with heat fluxes between the atmosphere, the surface skin layer and the material. The energy budget, in similar fashion to the PALM-LSM (Maronga and Bosveld, 2017), is expressed in the form:

$$C_0 \frac{dT_0}{dt} = R_n - H - G, \tag{1}$$

where C_0 is the heat capacity of the surface skin layer, T_0 is the temperature of the surface skin layer, R_n is the net radiation, H is the turbulent sensible heat flux near the surface and G is the heat flux from the surface skin layer into the ground or material (i.e. pavement, walls, roofs).

Geosci. Model Dev. Discuss., doi:10.5194/gmd-2017-61, 2017
Manuscript under review for journal Geosci. Model Dev.
Discussion started: 15 March 2017

Geoscientific Model Development Discussions

The calculation of the heat transfer H between the surface skin layer and the air is based on the equation:

$$H = ah(\Theta_1 - \Theta_0), \tag{2}$$

where Θ_0 is the potential temperature at the surface and Θ_1 is the potential temperature of the air layer adjacent to the surface. Further, h is the heat flux coefficient and a is an additional empirical parameter for fine tuning of modelled conditions. The coefficient h is parameterized according to Krayenhoff and Voogt (2007) for vertical surfaces, while for horizontal surfaces the parameterization of h follows the PALM-LSM formulation (Maronga and Bosveld, 2017) based on Monin-Obukhov similarity theory (Obukhov, 1971).

Heat transfer between surface skin layer and subsurface layers follows the general formulation for the heat flux G:

$$G = \Lambda(T_0 - T_{matter,1}), \tag{3}$$

where T_0 is the temperature of the surface skin layer, $T_{matter,1}$ is the temperature of the outermost layer of the material and Λ is the empirical heat conductivity between the skin layer and the material.

The calculation of heat transfer inside the material is achieved by using the Fourier law of diffusion which is also used for soil heat transfer in PALM's LSM. This approach has been generalized for different types of the material of pavements, walls, and roofs. The diffusion equation is solved numerically describing the heat transfer from the surface into the inner layers. Boundary conditions of the deepest layer are prescribed in the configuration for particular types of surfaces and are kept constant throughout the simulation. The ground heat flux calculated in the surface energy balance model serves as a boundary condition for the layer of air adjacent to the surface. In this version of the USM, the material is treated as homogeneous for all layers.

All non-linear terms in Eq. (1) are linearized to avoid the need of an iteration method to solve for the skin temperature. Equation (1) is then solved by PALM's default Runge-Kutta scheme. The near-surface heat fluxes are evaluated based on the new skin temperature value for horizontal and vertical surfaces.

2.2 Radiation processes in USM

2.2.1 General concept

The USM receives radiation from the standard PALM solar radiation model at the top boundary of the urban layer. Depending on the chosen radiation module in PALM, the separate direct and diffuse components of downward shortwave radiation flux may or may not be available. In the latter case a simple statistical splitting based on a clearness index is applied (Boland et al., 2008). The USM then adds a description of radiation processes in the urban canopy layer where multiple reflections are considered. The following processes are modelled for shortwave (SW) and longwave (LW) radiation:

- Radiation sources from the sun (SW direct and diffuse) and surface thermal emission (LW) using the relative position of the sun, surface temperature and shading according to urban-canopy geometry;
- Finitely iterated reflection of SW and LW radiation by real surfaces. Reflection is treated as diffuse;

Geosci. Model Dev. Discuss., doi:10.5194/gmd-2017-61, 2017
Manuscript under review for journal Geosci. Model Dev.
Discussion started: 15 March 2017

Geoscientific Model Development Discussions

- Absorption of radiation by individual grid cell surfaces (faces) based on surface properties (albedo and emissivity);
- Partial absorption of SW radiation by grid boxes containing plant canopy.

Some radiation-related processes were omitted at this stage for the sake of computability and efficiency, these include:

- Infinite reflection of radiation (after predefined number of reflections the remaining radiation is considered fully absorbed by the surface);
- Specular reflection (e.g. glass and polished surfaces);
- Absorption, emission, and scattering by air (considering short distances);
- For LW radiation, plant canopy is considered fully transparent;
- Thermal capacity of plant leaves: plant canopy is assumed to have the temperature of surrounding air. The energy from absorbed SW radiation heats the air mass directly.

2.2.2 Calculation of view factors and canopy sink factors

For the calculation of irradiation of each face from diffuse solar radiation, thermal radiation and reflected radiation, mutual visibility between faces of both real surfaces and virtual surfaces (top and lateral boundaries) is needed. It is calculated using a ray tracing algorithm. Since this process is computationally expensive and hard to parallelize (as rays can travel through the entire domain which is distributed on different processors), it is precomputed during the model initialization in the form of view factors (SVF) and plant-canopy sink factors (CSF). These factors also can be saved into a file and used for other simulations with the same surface geometry or for calculation of the mean radiant temperature (MRT) in the postprocessing.

For any two faces A and B with mutual visibility, the view factor $F_{A\to B}$ represents the fraction between that part of radiant flux from face A that strikes face B and the total radiant flux leaving face A. For infinitesimally small areas of A and B, a differential view factor can be written as:

$$F^d_{A\to B} = \frac{dF_{A\to B}}{d\mathcal{A}(B)} = \frac{\cos\theta_A \cos\theta_B}{\pi s^2}, \tag{4}$$

where $\mathcal{A}(B)$ is the surface area of face B, θ_A and θ_B are the angles between the respective face normals and the connecting ray, and s is the separation distance (ray length) (Fig. 1a). Under the assumption that the separation distance is much larger than grid resolution, differential view factors are precomputed for all mutually visible face centres. At the end, all the differential view factors for target face B are normalized using all visible source faces A:

$$\widehat{F}^d_{A\to B} = \frac{F^d_{A\to B}}{\sum_{A'} F^d_{A'\to B}\mathcal{A}(A')}. \tag{5}$$

This guarantees that, in total, no radiation is lost or created by simplification due to discretization. Since the part of face B's irradiance that comes from face A is computed as

$$J_{e,A\to B} = E_{e,A}\mathcal{A}(A)\widehat{F}^d_{A\to B}, \tag{6}$$

Geosci. Model Dev. Discuss., doi:10.5194/gmd-2017-61, 2017
Manuscript under review for journal Geosci. Model Dev.
Discussion started: 15 March 2017

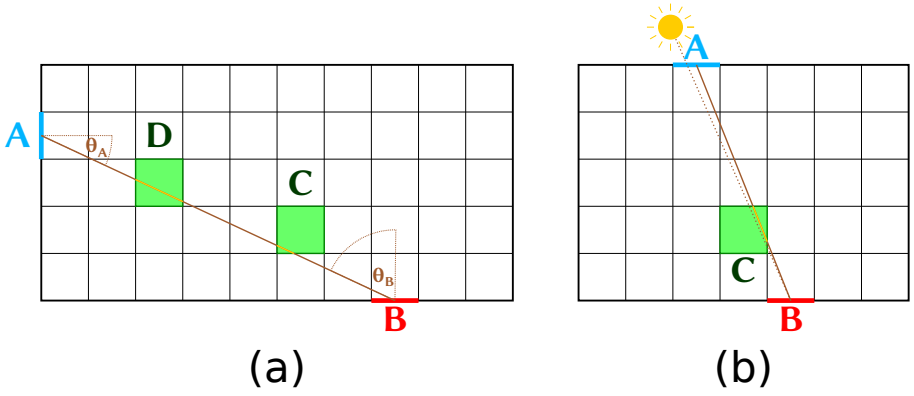

Figure 1. (a) View factor calculation (2-D simplification); (b) Direct solar irradiation

where $E_{e,A}$ is the radiosity of face A, we actually precompute and store the value of

$$SVF_{A\to B} = \mathcal{A}(A)\widehat{F}^{d}_{A\to B} \tag{7}$$

(internally called *irradiance factor*). In case the ray tracing algorithm encounters an obstacle (i.e. wall or roof), the view factor entry is not stored, indicating absence of mutual visibility between the two respective faces.

For every ray that crosses a grid box containing plant canopy (i.e. a partially opaque box), a ray canopy sink factor (RCSF) represents the proportion of the radiative flux carried by the ray at its origin that is absorbed within the respective grid box. For a ray $A \to B$ and a grid box C, the RCSF is calculated as

$$RCSF_{C,A\to B} = \left(1 - \sum_{D} RCSF_{D,A\to B}\right)\left(1 - e^{-\alpha a_C s_C}\right), \tag{8}$$

where a_C is the leaf area index of grid box C, s_C is the length of the ray's intersection with box C and α is the extinction coefficient. Summation is done for every plant-canopy-containing grid box D on the ray's path before reaching grid box C (Fig. 1a).

After the entire ray is traced, the total transmittance T of the ray $A \to B$ passing through plant canopy grid boxes C

$$T_{A\to B} = 1 - \sum_{C} RCSF_{C,A\to B} \tag{9}$$

is stored along with $SVF_{A\to B}$. Later in the modelling, when radiant flux transmitted through $SVF_{A\to B}$ is calculated, it is multiplied by $T_{A\to B}$ to account for the absorbed flux.

The actual radiant flux Φ_e received by the grid box C from the ray $A \to B$ is equal to

$$\Phi_{e,C,A\to B} = E_{e,A}\ SVF_{A\to B}\ \mathcal{A}(B)\ RCSF_{C,A\to B}. \tag{10}$$

Geosci. Model Dev. Discuss., doi:10.5194/gmd-2017-61, 2017
Manuscript under review for journal Geosci. Model Dev.
Discussion started: 15 March 2017

The radiosity $E_{e,A}$ of the source face is the only time-dependent variable in this equation. Therefore, the rest of this product can be precomputed during initialization and also summed up per source face in form of a canopy sink factor (CSF):

$$CSF_{C,A} = \sum_B SVF_{A\to B}\ \mathcal{A}(B)\ RCSF_{C,A\to B}. \tag{11}$$

CSF represents the ratio between the radiant flux absorbed within plant canopy box C originating from face A and the radiosity of face A.

2.2.3 Calculation of per-face irradiation

At each time step, the total irradiation of each face is computed iteratively, starting from the first pass of radiation from sources to immediate targets, followed by further reflections.

In the first step, the virtual surfaces (sky and boundary) are used as sources of radiation by representing components of diffuse shortwave solar radiation and longwave radiation from the sky. At this point, the real surfaces (wall facades, roofs, ground) are set to emit longwave radiation according to their surface temperature and emissivity. The precomputed view factors are then used to cast the shortwave and longwave radiation from source to target faces.

Solar visibility has to be calculated for the quantification of direct part of shortwave solar radiation. Solar angle is discretized for this purpose so that the solar ray always comes from the center of the virtual face at urban layer top or lateral boundary – see the real location of sun vs. discretized location (center of face A) at Fig. 1b. Ray tracing through entire model domain would be computationally expensive; on the other hand, the total transmittance stored alongside the precomputed view factor (see Eq. (9)) is readily available. If there is no such view factor entry, it means that the discretized ray path is blocked by a wall or roof and the target face receives no direct solar irradiation. For the purpose of calculating the actual amount of direct solar irradiation, an exact solar angle is used, not the discretized one.

After the first pass of radiation from the aforementioned sources to target surfaces has been computed, reflection is applied iteratively. At each iteration, a fraction of each surface's irradiation from the previous iteration is reflected and the remainder is considered absorbed. The reflected fraction is determined by the albedo for shortwave radiation and by the surface emissivity for longwave radiation, where the longwave reflectivity results from $(1-\textit{emissivity})$, according to Kirchhoff's law. The reflected part is then again distributed onto visible faces using the precomputed view factors. After the last iteration, all residual irradiation is considered as absorbed. The number of iterations is configurable and the amount of residual absorbed radiation can be displayed in the model output. In our experience, three to five iterations lead to negligible residue.

2.2.4 Absorption of radiation in plant canopy

For the initial radiation transfer and for all the reflection steps described in Sect. 2.2.3 a fraction of radiation flux absorbed by the plant canopy is calculated.

For diffuse and reflected shortwave radiation, the amount of radiation flux absorbed by each grid box with plant canopy is determined using the precomputed CSF and radiosity of the source face (i.e. reflected radiosity for a real surface or diffuse solar irradiance for a virtual surface, see Eq. (10)).

Geosci. Model Dev. Discuss., doi:10.5194/gmd-2017-61, 2017
Manuscript under review for journal Geosci. Model Dev.
Discussion started: 15 March 2017

Geoscientific Model Development Discussions

For the direct solar irradiance, the nearest precomputed ray path from the urban layer bounding box (represented by virtual face A in Fig. 1b) to the respective plant canopy grid box C is selected similarly as for the direct surface irradiation described in Sect. 2.2.3. In case the grid box C is fully shaded, no ray path is available. Otherwise the transmittance of the path is known. The absorbed direct solar flux for the grid box C is equal to

$$\Phi_{e,C} = E_{e,dir}\ T_{A\to C}\ \frac{\iint_b (1 - e^{-\alpha a_C s_b})\, db}{\mathcal{A}'_C}, \tag{12}$$

where $E_{e,dir}$ is the direct solar irradiance and $\mathcal{A}'_C$ is the cross-sectional area of C viewed from the direction of the solar radiation. The fraction in Eq. (12) represents the absorbed proportion of radiative flux averaged over each ray b that intersects the grid box C and is parallel to the direction of the solar radiation; s_b is the length of the intersection. Since all grid boxes have similar dimensions, this fraction is precomputed based on the solar direction vector at the beginning of each time step using discrete approximation.

Once the total absorbed radiative flux is known, it is stored as plant canopy heat rate for the respective grid box. Since the plant canopy is considered to have zero thermal capacity, all of the heating power is applied immediately to the grid box's air volume.

2.3 USM module integration into PALM

The USM was fully integrated into PALM following its modular concept as an optional module, and it directly utilizes the model values of wind flow, radiation, temperature, energy fluxes and other required values. The USM returns the predicted skin temperature and heat fluxes back to the PALM core, where they are subsequently considered in the corresponding prognostic equations.

Descriptions of real and virtual surfaces and their properties are stored in one dimensional arrays indexed to the 3D model domain. The crucial challenge of this part of the design is to ensure an efficient parallelization of the code, including an efficient handling and access of data stored in the memory during the simulation. The values are stored locally in particular processes of the Message Passing Interface (MPI[3]), corresponding to the parallelization of the PALM core. Necessary access to values stored in other processes is enabled by means of MPI routines including interfaces for one-sided MPI communication.

The configuration of the module is implemented in a separate configuration block compatible with other PALM modules, and the configuration options are described together with the USM input files in the module documentation. Variables for instantaneous and time-averaged outputs of the USM are integrated into PALM's standard 3D NetCDF output files, and they are configured in the same way as the rest of the model output variables. The configuration options as well as the structure of input and output files are described in the supplements to this article. The USM code has been integrated into the PALM codebase and is freely available (see section 6).

[3]http://mpi-forum.org

Geosci. Model Dev. Discuss., doi:10.5194/gmd-2017-61, 2017
Manuscript under review for journal Geosci. Model Dev.
Discussion started: 15 March 2017

2.4 Limitations

The present version of the USM describes only a portion of the processes taking place in urban environment. Limitations of the current version include:

- The model does not treat the reflective surfaces and windows.
- The material of walls is considered homogeneous and thus thermal conductivity of sandwich structure of insulated walls is not well described, as well as structure of pavements and streets.
- The indoor temperature is taken as constant during the simulation time.
- Plant canopies are considered transparent for long wave radiation.
- Evapotranspiration of the plant canopy is not modelled and surfaces are considered impervious to water.
- Anthropogenic heat is modelled only in the surface layer.
- Parameterizations of surface heat flux should be thoroughly tested for the conditions modelled by, and the resolution used in, the USM.

These issues are subjects of the ongoing improvements of the module inside the PALM community.

3 Evaluation and sensitivity test of USM

3.1 Observation campaign

A measurement campaign to evaluate the model was carried out at the crossroads of Dělnická street and Komunardů street in Prague, Czech Republic. This location is a case study area for urban heat island adaptation and mitigation strategies considered by the Prague Institute of Planning and Development. Figure 2 shows nine observation locations from which infrared spectrum images were taken. From eight of them (No. 1-7 and 9) the temperature of the wall on the opposite side of the street was measured and from one (No. 8) measurement of the ground temperature of the road was done. Measurements were conducted from 2 July 2015, 14:00 UTC to 3 July 2015, 17:00 UTC. Images were taken starting at observation location 1 every full hour and continuing through observation locations 2, 3, etc. This provided a series of 27 temperature snapshots per location with approximately 1 h time step. Exact time of taking a picture was used for further processing and evaluation of the model.

Temperature was measured by an infrared camera FLIR SC660 (FLIR, 2008) placed on a tripod stand at about 1.6 m above ground. The measurement accuracy for an object having a temperature within the range from $+5\ ^{\circ}\mathrm{C}$ to $+120\ ^{\circ}\mathrm{C}$, and given an ambient air temperature between $+9\ ^{\circ}\mathrm{C}$ and $+35\ ^{\circ}\mathrm{C}$, is $\pm 1\ ^{\circ}\mathrm{C}$ or $\pm 1\ \%$ of the reading. The camera offers a built-in emissivity correction option, which was not used for this study. Pictures in both the infrared and visible spectrum were taken simultaneously.

Geosci. Model Dev. Discuss., doi:10.5194/gmd-2017-61, 2017
Manuscript under review for journal Geosci. Model Dev.
Discussion started: 15 March 2017

Geoscientific Model Development Discussions
Open Access
EGU

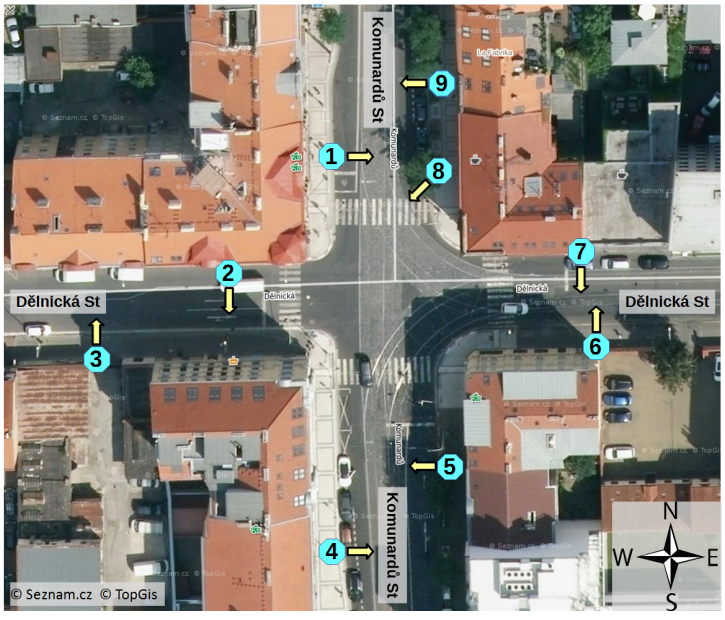

Figure 2. Observation locations. Arrows depict the orientation of the camera view. Url of the map: https://mapy.cz/s/12Qd8.

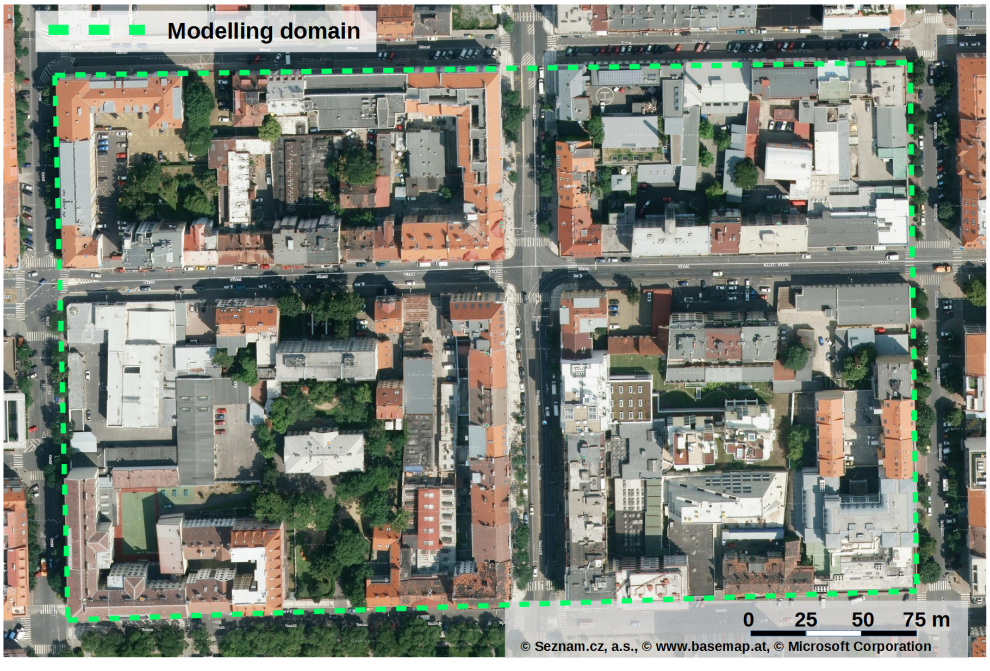

Figure 3. Aerial photo of the modelling domain.

Geosci. Model Dev. Discuss., doi:10.5194/gmd-2017-61, 2017
Manuscript under review for journal Geosci. Model Dev.
Discussion started: 15 March 2017

The pictures were postprocessed by: Firstly transforming the infrared pictures into a common temperature scale $+10\ ^{\circ}\mathrm{C}$ to $+60\ ^{\circ}\mathrm{C}$. Secondly, the pictures were transformed to correct for slight changes in camera position during measurement. Lastly, for each observation location, several evaluation points for comparison with model results were carefully selected to cover various surfaces types (material, colour, shading by existing trees, etc.) – see section 3.4.

Apart from infrared camera scanning, an indicative measurement of air temperature was performed at observation location 1. Temperature was measured at the edge of the pavement at about $2\ \mathrm{m}$ above ground and not in direct sunlight.

The timing of the measurement campaign was chosen to cover a typical summer heatwave episode. The weather during the campaign was influenced by a high-pressure system centred above the Baltic Sea. According to the Prague station Karlov ($4.3\ \mathrm{km}$ away), wind speed above rooftop was mostly below $2.5\ \mathrm{m\,s^{-1}}$ and often as low as $1\ \mathrm{m\,s^{-1}}$. Maximum measured wind speeds of 3–4 $\mathrm{m\,s^{-1}}$ were observed in the afternoons at the beginning and at the end of the campaign. The temperature exceeded $30\ ^{\circ}\mathrm{C}$ in the afternoon and dropped to $20\ ^{\circ}\mathrm{C}$ during the night. Sky was mostly clear with some high-latitude cirrus forming in the morning and afternoon on 3 July.

3.2 Model setup

To assess the validity of the model formulation and its performance in real conditions, the model was setup to simulate the measured summer episode described in section 3.1. The total simulation time span was 72 hours including 38 hour spin-up starting on 1 July 2015, 0:00 UTC. The model domain was set up to represent the crossroads of Dělnická and Komunardů in Prague (Fig. 3) with a horizontal domain size of $376\ \mathrm{m} \times 226\ \mathrm{m}$ and a resolution of $2.08\ \mathrm{m} \times 2.08\ \mathrm{m}$. The vertical grid spacing was $2.08\ \mathrm{m}$ within the first $50\ \mathrm{m}$ and above this level a vertical stretching factor of 1.08 between two adjacent levels was used. The total domain height then was $2364\ \mathrm{m}$.

The lateral boundary conditions were set as cyclic, i.e. the streets are treated as if being infinite. This is a reasonable approximation since the surrounding area has similar characteristics as the model domain and effects from outside the domain can be considered to be of minor importance compared to those imposed by the local forcing. At the top of the domain the Neumann boundary condition was applied. The bottom boundary condition is driven by ground heat flux – see section 2.1. The large-scale forcing option of PALM was used taking temperature and velocity tendencies from the mesoscale numerical weather prediction model WRF (Skamarock et al., 2008). The main WRF integration domain covered the whole Europe with $9\ \mathrm{km}$ horizontal resolution and 49 vertical levels and a nested domain covering the Czech Republic with $3\ \mathrm{km}$ horizontal resolution. Standard physics parameterizations were used including the RRTMG radiation scheme, Monin-Obukhov similarity surface layer scheme and Noah land surface model (Tewari et al., 2004) without its urban canopy model. Such a configuration corresponds to an operational run of the Medard prediction system[4].

[4] http://medard-online.cz/

Geosci. Model Dev. Discuss., doi:10.5194/gmd-2017-61, 2017
Manuscript under review for journal Geosci. Model Dev.
Discussion started: 15 March 2017

Geoscientific Model Development Discussions
Open Access
EGU

3.3 Input data for USM

3.3.1 Surface and material parameters

Solving the USM energy balance equations requires a number of surface (albedo, emissivity, roughness and thermal conductivity between air and surface) and material (thermal capacity and volumetric thermal conductivity) input parameters to be set in the model accurately.

When going to such high resolution as in our test case (~ 2 m), the urban surfaces and wall materials become very heterogeneous, therefore any bulk parameter setting would be inadequate. We opted instead for detailed setting of these parameters wherever possible. To obtain these data, a supplemental onsite data collection campaign was carried out and a detailed database of geospatial data was created. This includes information on wall, ground and roof materials and colours which was used to estimate surface and material properties. Building heights were available from a Prague 3D model (Prague Institute of Planning and Development[5]). The urban vegetation (trees) was described by its position, height and width of the treetop and leaf area density.

3.3.2 Anthropogenic heat

Anthropogenic heat sources for our particular case are dominated by heat from fuel combustion in cars. Other sources of anthropogenic heat in our simulation are omitted. This heat is considered as an additional heat flux through the respective surface. The calculation of traffic heat flux is based on the heat flux released by cars per meter of their trajectory (Sailor and Lu, 2004). The heat produced by the cars along their trajectories is subsequently spatially distributed into street zones of the traffic flow and temporally distributed using prescribed hourly factors. Traffic intensities and hourly traffic factors are based on annual traffic census data. Values of anthropogenic heat in the peak traffic hour were on average 47 W m^{-2} (maximum 142 W m^{-2}) and on average 3 W m^{-2} (maximum 10 W m^{-2}) when the traffic was the lowest.

3.4 Results

In this section a detailed comparison of the results from PALM model with the USM module switched on (hereafter referred to as PALM-USM) and measurements taken during the observation campaign is presented. For the interpretation of the data it should be noted that the time of the sunset was 19:15 UTC on 2 July 2015, time of the sunrise 2:58 UTC and time of the noon 11:06 UTC on 3 July[6].

Figure 4 shows surface temperatures for the whole modelling domain at 12:00 UTC, demonstrating different heating of facades due to different surface and material properties. For example, see the south oriented buildings along Dělnická street (cf. also Fig. 3), where the walls have markedly different temperature, although they are approximately equally irradiated by the sun. Further, the effect of vegetation shading is clearly visible (see Fig 4). It is also possible to demonstrate the effect of transforming the real urban geometry into the regular grid (approximately 2 m resolution in our case): e.g. a slanted roof

[5]http://www.geoportalpraha.cz
[6]http://www.timeanddate.com

Geosci. Model Dev. Discuss., doi:10.5194/gmd-2017-61, 2017
Manuscript under review for journal Geosci. Model Dev.
Discussion started: 15 March 2017

Geoscientific Model Development Discussions
Open Access
EGU

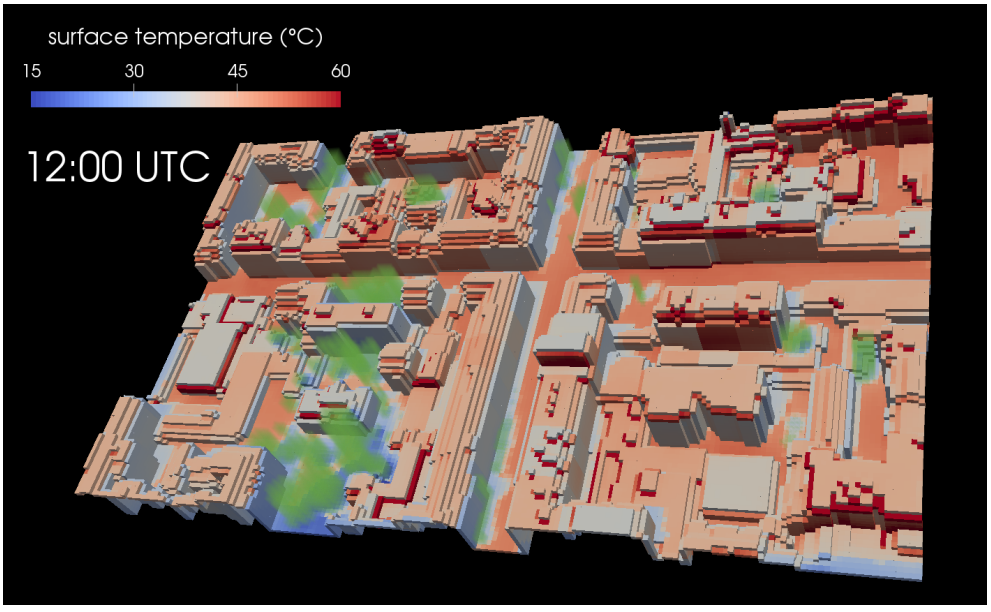

Figure 4. Surface temperatures at 12:00 UTC. Green areas represent vegetation (trees).

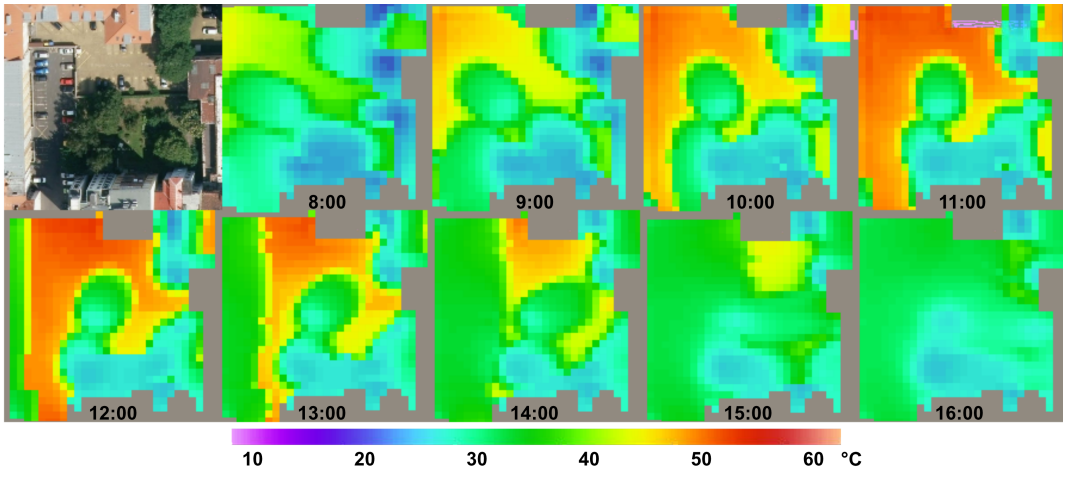

Figure 5. Aerial photo and modelled surface temperature of courtyard in the south-west corner of the domain for hours from 8:00 UTC to 16:00 UTC on 3 July.

surface is represented as "sequence of steps" and reflection of radiation can then lead to unrealistic increases in temperature in some cases. Variations in subgrid sized facades (balconies, mouldings, etc.), which can have local shading effect cannot be captured. Figure 5 shows the diurnal course of the surface temperature of the pavement in the closed courtyard near the north-west corner of the domain and it illustrates the effects of tree shading.

Geosci. Model Dev. Discuss., doi:10.5194/gmd-2017-61, 2017
Manuscript under review for journal Geosci. Model Dev.
Discussion started: 15 March 2017

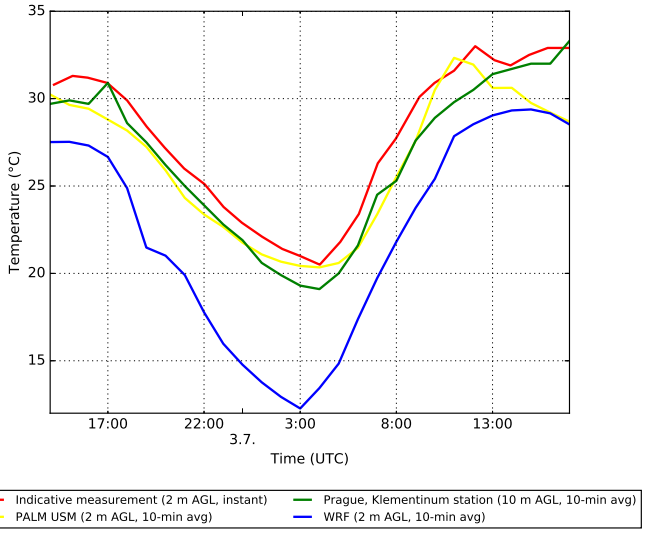

Figure 6. Comparison of WRF, measured and modelled air temperatures at 2 m AGL.

Figure 6 shows the temperature course calculated by the PALM-USM at observation location 1. This temperature is compared to the indicative measurement taken at the same place and to the automatic weather station measurement on the north facing wall of the courtyard of Klementinum complex in the historical centre of Prague, which is located about 3 km away. Temperature output from the WRF model, used as forcing data to calculate temperature tendencies in PALM due to large-scale advection and subsidence, is also shown. Apparently, the air temperature at street level predicted by PALM-USM is in remarkable agreement with both the measurements at location 1 and at Klementinum, while WRF suggests up to 7 °C lower temperature (around 3:00 UTC). PALM-USM thus seems to be able to correct for the bias of WRF, which is indicative of improved representation of the urban heat island effect in PALM-USM

Comparison of on-site measurements of surface temperatures captured by the infrared camera and the modelled values is displayed in Figs. 7 to 11. In general, PALM-USM captures the observed patterns and values quite well. More detailed conclusions do not reflect only the physical formulation of USM, but to a large extent also the surface and material parameters used:

- The modelled wall surface temperature drops more rapidly than the measured temperature after the sunset. This leads to a systematic underestimation of wall temperature by about 2 °C during the night time. The only exceptions were at evaluation points 4–7 (Fig. 7), which represent recently built and well insulated building walls that cool more rapidly at night than the facade of an old brick house (evaluation points 1–3 in Fig. 7). This leads to a difference in measured temperature by about 4 °C. In model configuration, walls corresponding to the evaluation points 3 and 4 in Fig. 7, although having different category, are described with almost identical surface and material parameters (the only difference is the albedo, which is set to 0.75 for the new and 0.6 for the old building, and the wall thickness of 0.3 m for the new and

Geosci. Model Dev. Discuss., doi:10.5194/gmd-2017-61, 2017
Manuscript under review for journal Geosci. Model Dev.
Discussion started: 15 March 2017

Geoscientific Model Development Discussions
Open Access
EGU

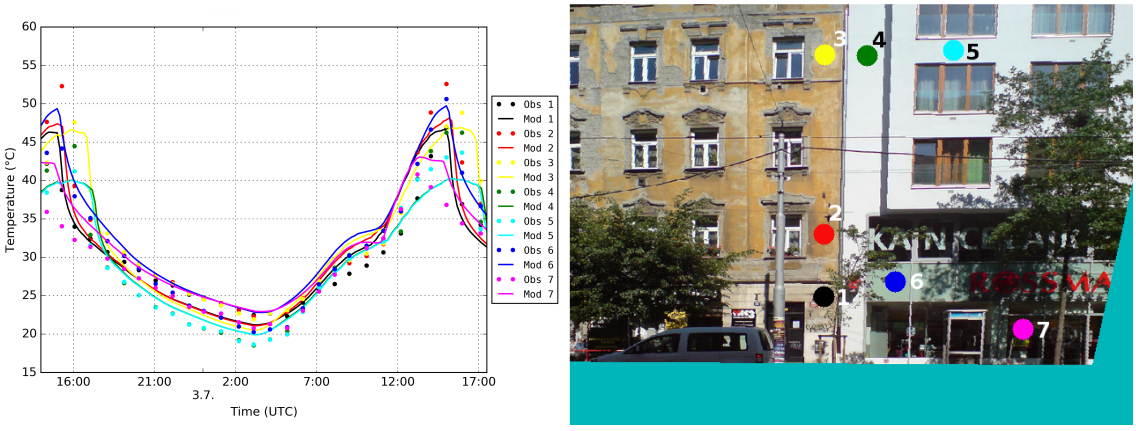

Figure 7. Measurements from the observation location 4 (west facing wall).

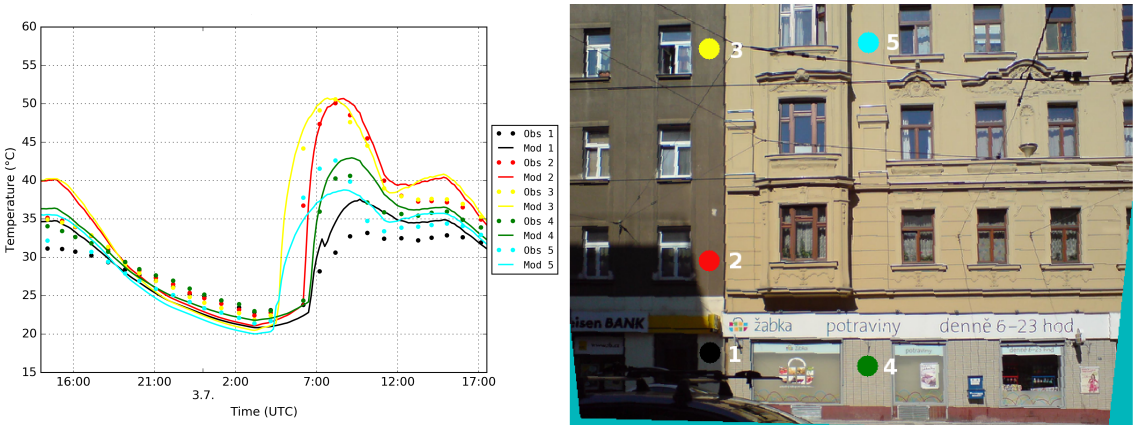

Figure 8. Measurements from the observation location 5 (east facing wall).

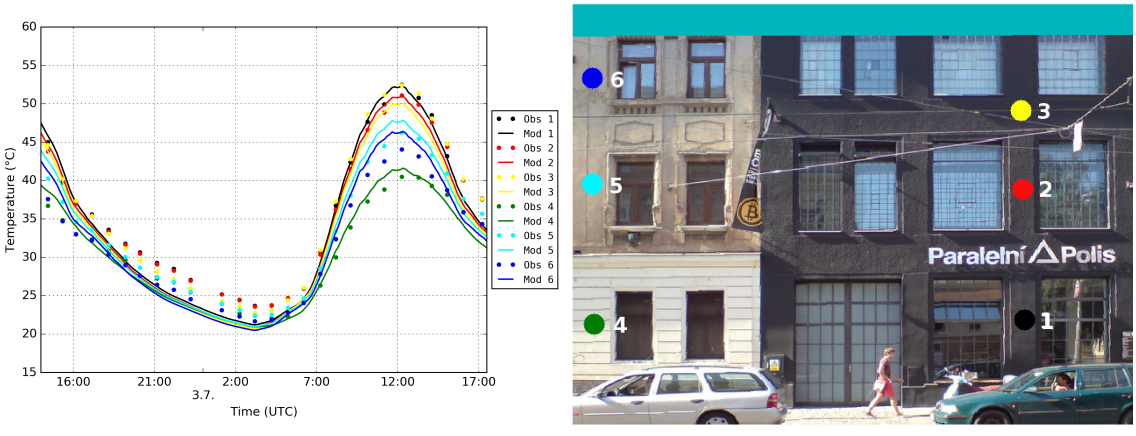

Figure 9. Measurements from the observation location 6 (south facing wall).

Geosci. Model Dev. Discuss., doi:10.5194/gmd-2017-61, 2017
Manuscript under review for journal Geosci. Model Dev.
Discussion started: 15 March 2017

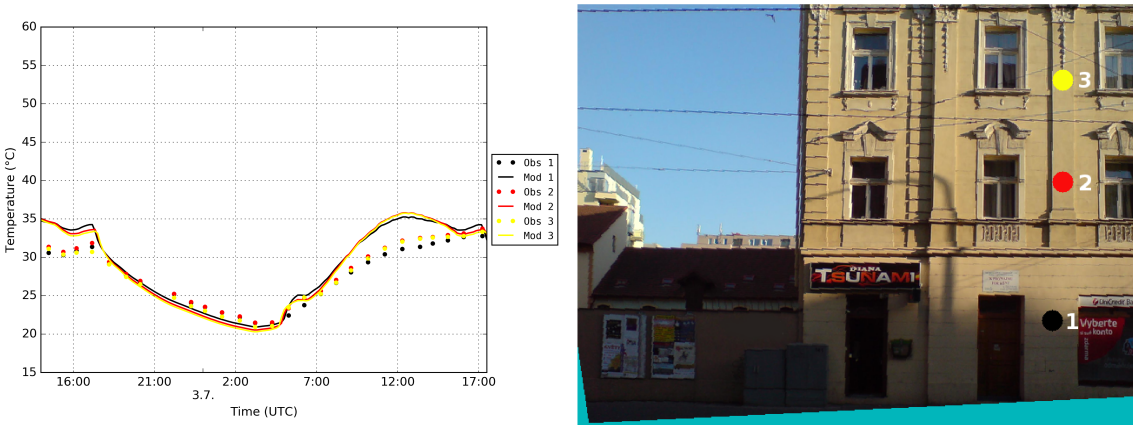

Figure 10. Measurements from the observation location 7 (north facing wall).

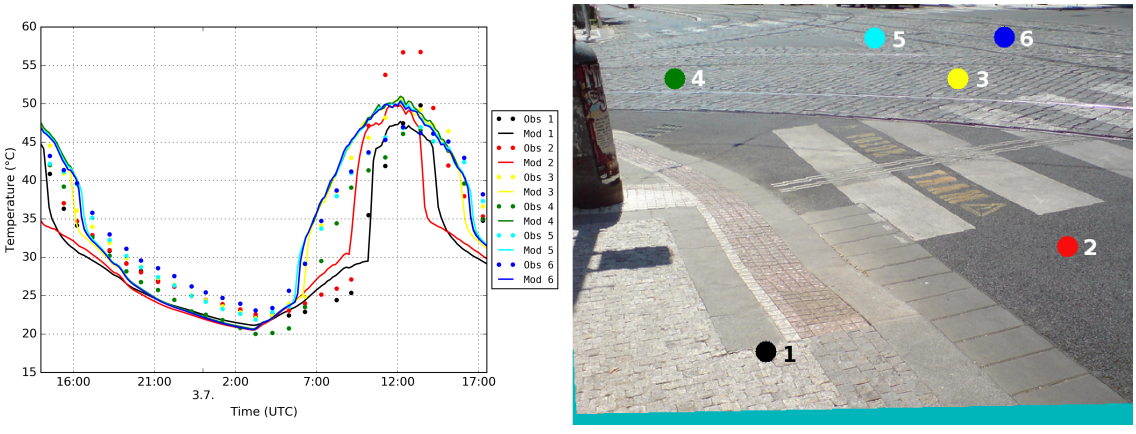

Figure 11. Measurements from the observation location 8 (crossroads – ground).

0.35 m for the old building). This results in very similar modelled surface temperatures at night and points towards an underestimation of the heat capacity and/or the overestimation of the skin conductivity. It also reflects the importance of correctly setting surface and material parameters.

– The model systematically overestimates temperatures on the north facing walls when the opposite walls are fully irradiated by the sun (Fig. 10, 8:00–14:00 UTC). The same effect is observed on the east facing wall (Fig. 8, 12:00–15:00 UTC) and the west facing wall (Fig. 7, 7:00–10:00 UTC). This may have several possible reasons e.g. underestimated heat capacity of the wall or that only diffuse reflection is considered (direct solar radiation incident on the windows is not distributed properly). Further testing needs to be done in order to clarify this effect.

Geosci. Model Dev. Discuss., doi:10.5194/gmd-2017-61, 2017
Manuscript under review for journal Geosci. Model Dev.
Discussion started: 15 March 2017

Geoscientific Model Development Discussions

– The temporal evolution of temperature for the east and west facing walls is less smooth around the noon when shading by bay windows, balustrades and other facade unevenness plays a key role. These effects are not captured by the model due to its resolution (e.g. Fig. 8, evaluation point 5).

– The highest measured temperatures of the asphalt ground surface (Fig. 11, evaluation point 2) are much higher (up to 7 °C) than modelled ones. This probably points to the fact that material parameter settings for this surface may have some deficiencies.

3.5 Sensitivity test

A simulation to quantify the effect of USM on PALM results was performed with the USM module switched off (PALM-noUSM). This setup can be viewed as forming a purely dynamical model without effects of radiation and heat fluxes on model dynamics. Figure 12 shows the horizontal view of the vertical velocity field at 10 m above ground level and at the first model level above the rooftop (37 m AGL). Pictures correspond to 9:00 UTC, when east facing walls had been already fully irradiated and heated up by the sun for about 2.5 hours. It can be seen that heat flux warming the air on the east facing wall (cf. also Figs. 4 and 2) changes the orientation of the street vortex perpendicular to the street axis as rising warm air parcels near the east facing walls dominate the flow circulation. Also the structure of the velocity field above the rooftop changes completely when radiation and heat fluxes are taken into account (Figs. 12 and 13), which is related to a transformation from a purely neutral boundary layer to convective conditions.

In order to examine the effect of the interactive wall temperature, calculated by the USM, on the temporal variability of vertical velocity, its time series in observation location 1 (cf. Fig. 2) in the model grid right next to the wall are shown (Fig. 14). This east facing wall was fully irradiated by the sun from 6:30 to 10:30 UTC. Compared to the PALM-noUSM simulation, the radiation effect in this time of the day led to positive velocities with the magnitude of change between 0.5–1 $\mathrm{m\ s^{-1}}$.

4 Computational aspects

The correct functionality and computational efficiency of the implementation of USM was verified in various environments. The tested configurations varied in processor type (Intel[7], AMD[8]), compiler (GNU[9], PGI[10], Intel[11]), implementation of MPI (MVAPICH2[12], IMPI[13]), and other aspects. The comparison presented in this chapter was performed on the supercomputer Salomon[14] with Intel C and Fortran compilers and Intel MPI (2016 versions for all). The setup of the model corresponds to the setup described in Sect. 3.2.

[7] https://ark.intel.com/
[8] http://www.amd.com/en-us/products/processors
[9] https://gcc.gnu.org/
[10] http://www.pgroup.com/
[11] https://software.intel.com/en-us/intel-compilers
[12] http://mvapich.cse.ohio-state.edu/
[13] https://software.intel.com/en-us/intel-mpi-library
[14] https://docs.it4i.cz/salomon/introduction

Geosci. Model Dev. Discuss., doi:10.5194/gmd-2017-61, 2017
Manuscript under review for journal Geosci. Model Dev.
Discussion started: 15 March 2017

Geoscientific Model Development Discussions

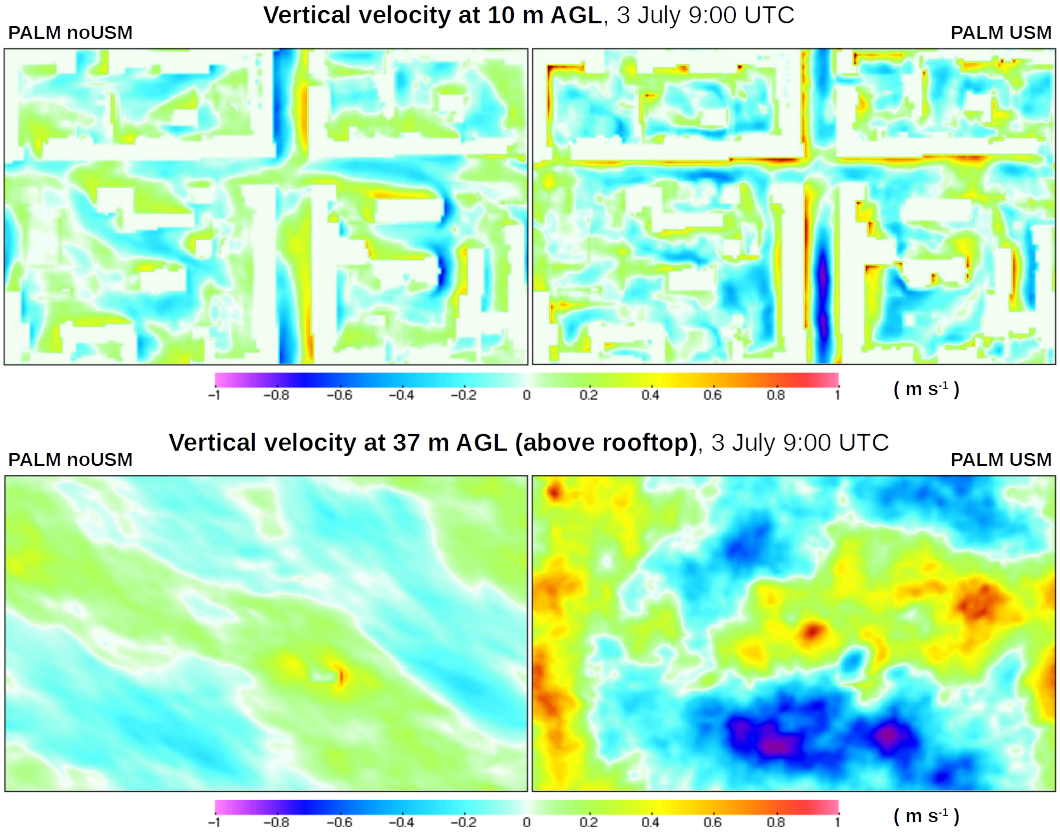

Figure 12. Horizontal view of vertical velocity field. Simulation without USM (left) and with USM (right).

Figure 15a shows the comparison of the total CPU time of the model run and the CPU time needed for particular chosen subroutines. Almost all of the total time is spent on time stepping. The direct expense of the USM can be split into three parts: the time spent in initialization routines of the USM at the start of the model run, the time needed for calculation of the urban radiation model and finally the time of remaining USM processes, particularly the energy balance and the material thermal diffusion. The total increase of the calculation time with USM switched on is about 25 % (29 % with plant canopy). However, the direct USM calculation cost presents only about 2 % (4 % with plant canopy) of the total calculation time. The rest of the increase can be attributed to the raised turbulent flow which results in decreased time step. Figure 15b shows the detailed comparison of USM processes. The initialization time of the USM is dominated by the calculation of SVF and CSF and about half of this calculation is spent with one-sided MPI communication in case of the run with plant canopy. The utilization of one-sided MPI routines can be avoided by distributing the global leaf area density (LAD) array into all MPI processes by setting the model configuration parameter usm_lad_rma to false, which reduces the time spent in USM initialization process and markedly improves the scaling behaviour.

Geosci. Model Dev. Discuss., doi:10.5194/gmd-2017-61, 2017
Manuscript under review for journal Geosci. Model Dev.
Discussion started: 15 March 2017

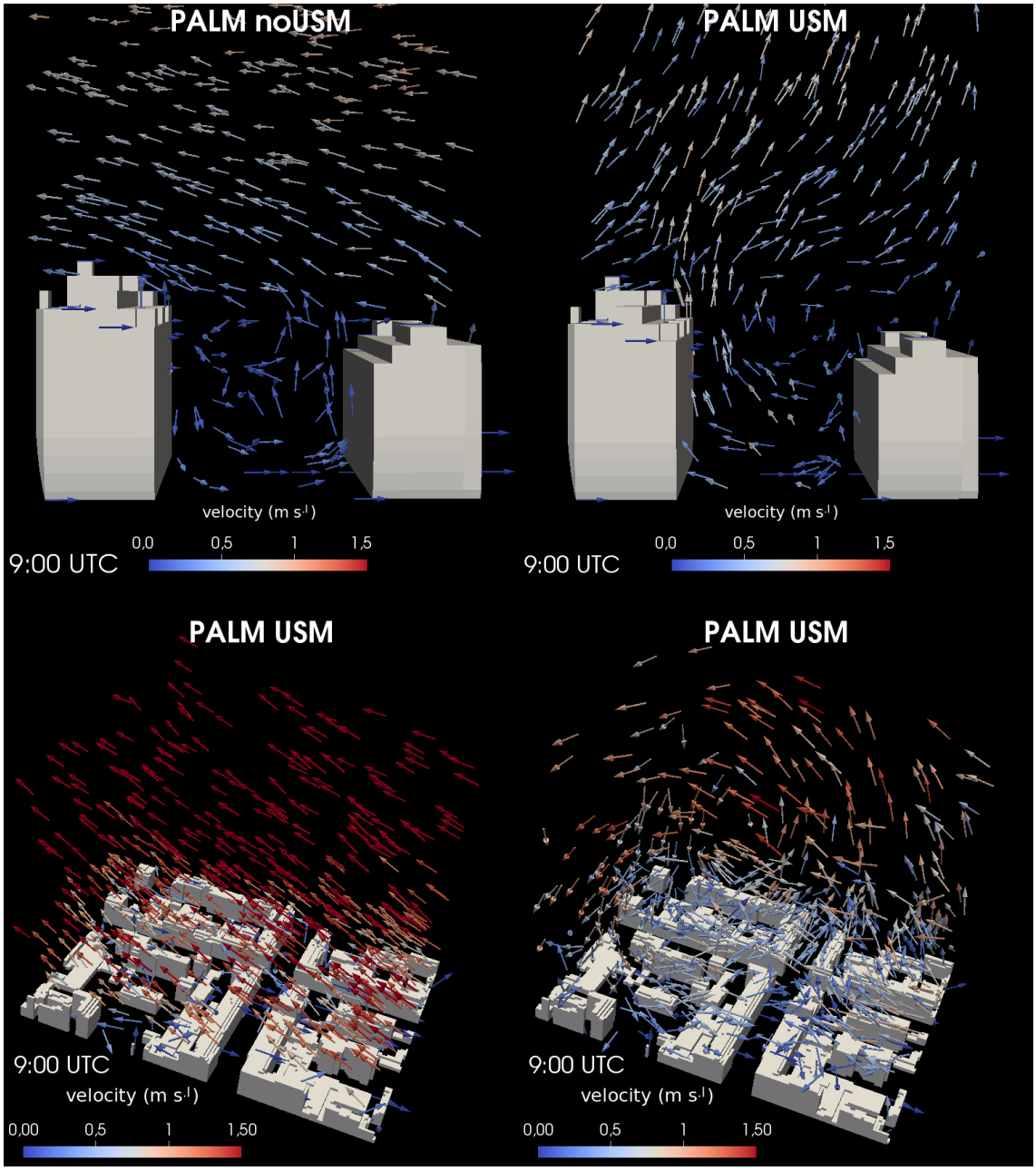

Figure 13. Velocity field. Simulation without USM (left) and with USM (right). Top: view from the crossroad towards the north. Bottom: complex view of the bottom part of the modelling domain.

Geosci. Model Dev. Discuss., doi:10.5194/gmd-2017-61, 2017
Manuscript under review for journal Geosci. Model Dev.
Discussion started: 15 March 2017

Geoscientific Model Development Discussions

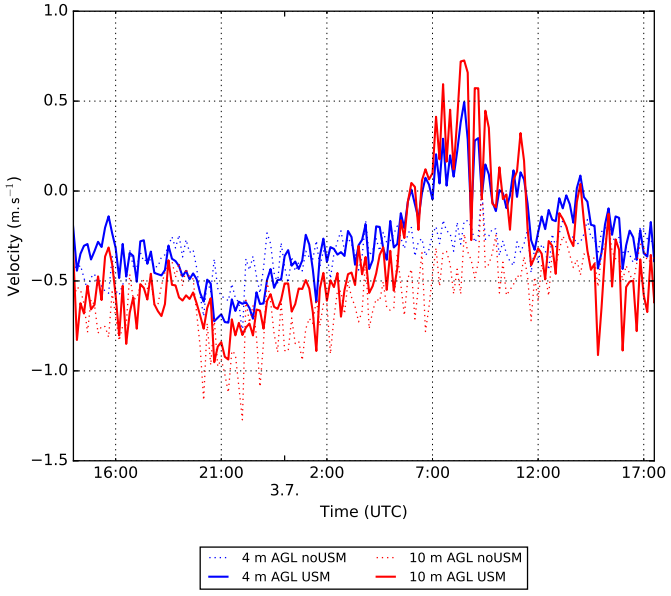

Figure 14. Time variability of vertical velocity at observation location 1. USM: simulation with urban model, noUSM: simulation without urban model.

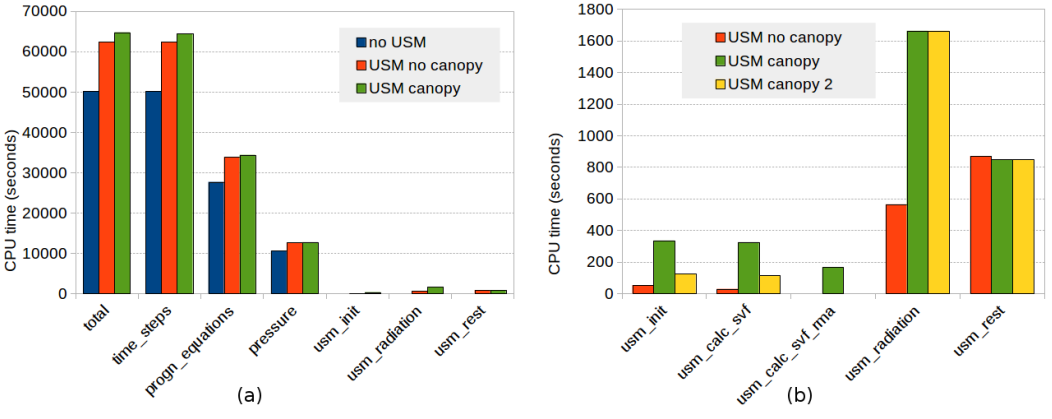

Figure 15. Comparison of duration of the model run and time spent in chosen subprocesses of the model (a) and detailed comparison of parts of USM model (b). Meaning of data series: "no USM" the run of PALM with USM switched off, "USM no canopy" the run with USM with no plant canopy, "USM canopy" run with USM and plant canopy, "USM canopy 2" the same run with the model configuration option usm_lad_rma turned off. Meaning of items: *total* – total CPU time of the model run, *time_steps* – time spent in time stepping, *progn_equations* – evaluation of all prognostic equations, *pressure* – pressure calculation, *usm_init* – initialization routines of USM, *usm_radiation* – calculation of USM radiation model, *usm_rest* – remaining USM processes (particularly energy balance and material thermal diffusion), *usm_calc_svf* – calculation of SVF and CSF, *usm_calc_svf_rma* – time spent with one-sided MPI communication.

Geosci. Model Dev. Discuss., doi:10.5194/gmd-2017-61, 2017
Manuscript under review for journal Geosci. Model Dev.
Discussion started: 15 March 2017

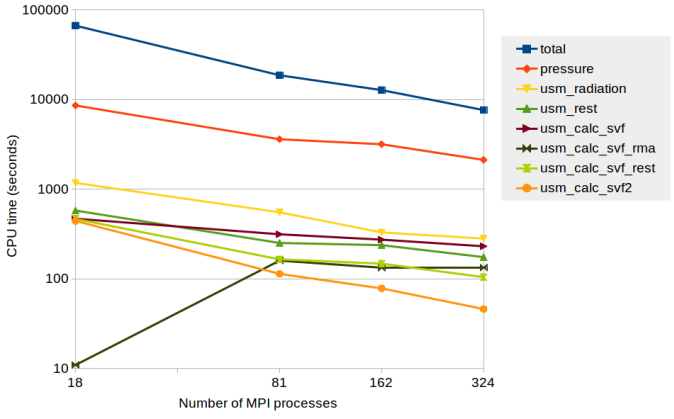

Figure 16. Comparison of the calculation time spent in model PALM-USM and in its chosen parts for various number of cores. Meaning of items is the same as in Fig. 15, additionally *usm_calc_svf_rest* shows the difference *usm_calc_svf* − *usm_calc_svf_rma* and *usm_calc_svf2* depicts *usm_calc_svf* in case of the run with option usm_lad_rma set to false.

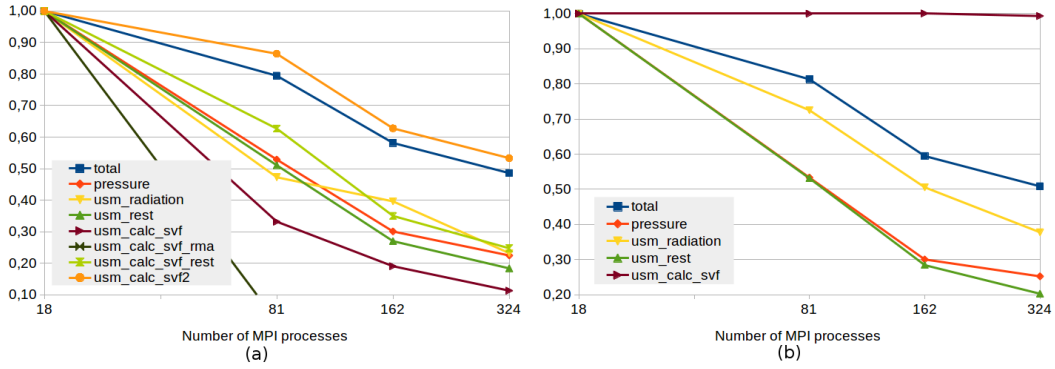

Figure 17. Effectiveness of parallelization of chosen subroutines: (a) simulation with plant canopy, (b) without plant canopy. Meaning of the items is the same as in Fig. 16.

The effectiveness of the parallelization had been tested for number of MPI processes in range from 18 to 324 for the simulation length 24 hours and the results are shown in Figs. 16 and 17. Figure 16 compares the CPU time needed for calculation of whole model PALM-USM and its chosen individual parts. Figures 17a and 17b show the effectiveness of the parallelization relative to a run with 18 processes for simulation with and without calculation of plant canopy, respectively. The graphs suggest that time-stepping routines *usm_radiation* and *usm_rest* scale similarly to calculation of the pressure which is the most time consuming individual process of the model PALM. The calculation of SVF during initialization phase scales excellently in the tested range according to Fig. 17b. Scaling of the calculation of CSF is on a par with the whole model PALM for configuration with the LAD array distributed into all processes (Fig. 17a, item *usm_calc_svf2*) while scaling of the *usm_calc_svf* is limited by latency of one-sided MPI operations implemented by an Infiniband RMA backend (Fig. 16, *usm_calc_svf_rma*). (Note that

the run with 18 processes fits into one node of the computational cluster and all MPI communication is done through a shared memory backend in our setup.) On the other hand, it also suggests that the computation of CSF can scale well when the computational domain extends. However, the testing domain is relatively small and additional tests with larger domains are needed to extract deeper insight into performance and scaling of PALM-USM.

5 Conclusions

The new model of energy processes in urban environment was developed and integrated into the PALM model as a switchable module USM. The USM utilizes meteorological values calculated by PALM, and provides the surface temperatures and heat fluxes to the other PALM processes. The model was evaluated against data from a measurement campaign in Prague (Czech Republic). The results are in good agreement with observations for our test case. The differences can be attributed to the grid discretization, and inaccurate description of the urban parameters as well as to some limitations of the current version of the model. Addressing these limitations is a subject of current and future development inside the PALM community. USM shows very moderate computational demand in the context of PALM's other processes. Most of the additional computational time with USM enabled can be attributed to increased turbulent flow leading to a shortened model time step. The PALM-USM model provides a new useful tool for climatology studies of urbanized areas, and has now been successfully used to simulate urban development scenarios for the city of Prague.

6 Code availability

The USM code is freely available and it is distributed under the GNU General Public License v3[15] . Its source code is a part of PALM and it can be downloaded from the PALM web page[16] via PALM SVN web interface[17] since PALM SVN revision 2008.

Competing interests. The authors declare that they have no conflict of interest.

Acknowledgements. This work was done within the UrbanAdapt project (EHP-CZ02-OV-1-036-2015) supported by grant from Iceland, Liechtenstein and Norway (http://urbanadapt.cz/en). This work was also supported by the Institute of Computer Science Academy of Sciences of Czech Republic with RVO:67985807. Some of the simulations were done on the supercomputer Salomon, which was supported by The Ministry of Education, Youth and Sports from the Large Infrastructures for Research, Experimental Development and Innovations project IT4Innovations National Supercomputing Center – LM2015070. Authors would like to thank Linton Corbet for language revisions and useful comments. We also would like to thank to the coordinator of the UrbanAdapt project Global Change Research Institute (CzechGlobe) for

[15] http://www.gnu.org/copyleft/gpl.html
[16] http://palm.muk.uni-hannover.de
[17] http://subversion.apache.org

Geosci. Model Dev. Discuss., doi:10.5194/gmd-2017-61, 2017
Manuscript under review for journal Geosci. Model Dev.
Discussion started: 15 March 2017

lending IR camera and František Zemek for his help with observation campaign. Finally, authors would like to thank to the UrbanAdapt project partner Prague Institute of Planning and Development for providing geographical data and also to the ATEM company for its help with the data processing.

References

Arakawa, A. and Lamb, V. R.: Computational Design of the Basic Dynamical Processes of the {UCLA} General Circulation Model, in: General Circulation Models of the Atmosphere, edited by Chang, J., vol. 17 of *Methods in Computational Physics: Advances in Research and Applications*, pp. 173–265, Elsevier, 1977.

Arnfield, A. J.: Two decades of urban climate research: a review of turbulence, exchanges of energy and water, and the urban heat island, Int. J. Climatol., 23, 1–26, doi:10.1002/joc.859, 2003.

Balsamo, G., Beljaars, A., Scipal, K., Viterbo, P., van den Hurk, B., Hirschi, M., and Betts, A. K.: A Revised Hydrology for the ECMWF Model: Verification from Field Site to Terrestrial Water Storage and Impact in the Integrated Forecast System, J. Hydrometeorol., 10, 623–643, doi:10.1175/2008JHM1068.1, 2009.

Boland, J., Ridley, B., and Brown, B.: Models of diffuse solar radiation, Renew. Energy, 33, 575–584, 2008.

Clough, S., Shephard, M., Mlawer, E., Delamere, J., Iacono, M., Cady-Pereira, K., Boukabara, S., and Brown, P.: Atmospheric radiative transfer modeling: a summary of the AER codes, J. Quant. Spectrosc. Ra., 91, 233–244, doi:http://dx.doi.org/10.1016/j.jqsrt.2004.05.058, 2005.

Deardorff, J. W.: Stratocumulus-capped mixed layers derived from a three-dimensional model, Bound.-Lay. Meteorol., 18, 495–527, doi:10.1007/BF00119502, 1980.

Ehrhard, J., Khatib, I. A., Winkler, C., Kunz, R., Moussiopoulos, N., and Ernst, G.: The microscale model MIMO: Development and assessment, J. Wind Eng. Ind. Aerod., 85, 163–176, 2000.

ENVI-met, 2009: ENVI-met 3.1 Manual Contents, http://www.envi-met.info/documents/onlinehelpv3/helpindex.htm, last access: September 2016, 2009.

FLIR, 2008: FLIR SC660 R&D INFRARED CAMERA SYSTEM. Product leaflet, http://www.flir.com/assets/6e002ff6acaa46a599ce08197091e01a.pdf, last access: September 2016, 2008.

Heus, T., van Heerwaarden, C. C., Jonker, H. J. J., Pier Siebesma, A., Axelsen, S., van den Dries, K., Geoffroy, O., Moene, A. F., Pino, D., de Roode, S. R., and Vilà-Guerau de Arellano, J.: Formulation of the Dutch Atmospheric Large-Eddy Simulation (DALES) and overview of its applications, Geosci. Model Dev., 3, 415–444, doi:10.5194/gmd-3-415-2010, 2010.

Järvi, L., Grimmond, C. S. B., and Christen, A.: The Surface Urban Energy and Water Balance Scheme (SUEWS): Evaluation in Los Angeles and Vancouver, J. Hydrol., 411, 219–237, doi:http://dx.doi.org/10.1016/j.jhydrol.2011.10.001, 2011.

Krayenhoff, E. S. and Voogt, J. A.: A microscale three-dimensional urban energy balance model for studying surface temperatures, Bound.-Lay. Meteorol., 123, 433–461, doi:10.1007/s10546-006-9153-6, 2007.

Lindberg, F., Holmer, B., and Thorsson, S.: SOLWEIG 1.0 – Modelling spatial variations of 3D radiant fluxes and mean radiant temperature in complex urban settings, Int. J. Biometeorol., 52, 697–713, doi:10.1007/s00484-008-0162-7, 2008.

Maronga, B. and Bosveld, F. C.: Key parameters for the life cycle of nocturnal radiation fog: a comprehensive large-eddy simulation study, Q. J. Roy. Meteor. Soc., submitted, 2017.

Maronga, B., Gryschka, M., Heinze, R., Hoffmann, F., Kanani-Sühring, F., Keck, M., Ketelsen, K., Letzel, M. O., Sühring, M., and Raasch, S.: The Parallelized Large-Eddy Simulation Model (PALM) version 4.0 for atmospheric and oceanic flows: model formulation, recent developments, and future perspectives, Geosci. Model Dev., 8, 2515–2551, doi:10.5194/gmd-8-2515-2015, 2015.

Masson, V.: A Physically-Based Scheme For The Urban Energy Budget In Atmospheric Models, Boundary-Layer Meteorology, 94, 357–397, doi:10.1023/A:1002463829265, 2000.

Matzarakis, A., Rutz, F., and Mayer, H.: Modelling radiation fluxes in simple and complex environments: basics of the RayMan model, Int. J. Biometeorol., 54, 131–139, doi:10.1007/s00484-009-0261-0, 2010.

Mirzaei, P. A.: Recent challenges in modeling of urban heat island, Sustainable Cities and Society, 19, 200–206, doi:http://dx.doi.org/10.1016/j.scs.2015.04.001, 2015.

Mirzaei, P. A. and Haghighat, F.: Approaches to study Urban Heat Island – Abilities and limitations, Build. Environ., 45, 2192–2201, doi:http://dx.doi.org/10.1016/j.buildenv.2010.04.001, 2010.

Moeng, C.-H. and Wyngaard, J. C.: Spectral Analysis of Large-Eddy Simulations of the Convective Boundary Layer, J. Atmos. Sci., 45, 3573–3587, doi:10.1175/1520-0469(1988)045<3573:SAOLES>2.0.CO;2, 1988.

Moonen, P., Defraeye, T., Dorer, V., Blocken, B., and Carmeliet, J.: Urban Physics: Effect of the micro-climate on comfort, health and energy demand, Frontiers of Architectural Research, 1, 197–228, doi:http://dx.doi.org/10.1016/j.foar.2012.05.002, 2012.

Musy, M., Malys, L., Morille, B., and Inard, C.: The use of SOLENE-microclimat model to assess adaptation strategies at the district scale, Urban Climate, 14, Part 2, 213–223, doi:http://dx.doi.org/10.1016/j.uclim.2015.07.004, 2015.

Obukhov, A. M.: Turbulence in an atmosphere with a non-uniform temperature, Bound.-Lay. Meteorol., 2, 7–29, doi:10.1007/BF00718085, 1971.

Oke, T. R.: The Heat Island of the Urban Boundary Layer: Characteristics, Causes and Effects, pp. 81–107, Springer Netherlands, Dordrecht, doi:10.1007/978-94-017-3686-2_5, 1995.

Saiki, E. M., Moeng, C.-H., and Sullivan, P. P.: Large-Eddy Simulation Of The Stably Stratified Planetary Boundary Layer, Bound.-Lay. Meteorol., 95, 1–30, doi:10.1023/A:1002428223156, 2000.

Sailor, D. J. and Lu, L.: A top-down methodology for developing diurnal and seasonal anthropogenic heating profiles for urban areas, Atmos. Environ., 38, 2737–2748, doi:http://dx.doi.org/10.1016/j.atmosenv.2004.01.034, 2004.

Schlünzen, K. H., Hinneburg, D., Knoth, O., Lambrecht, M., Leitl, B., López, S., Lüpkes, C., Panskus, H., Renner, E., Schatzmann, M., Schoenemeyer, T., Trepte, S., and Wolke, R.: Flow and Transport in the Obstacle Layer: First Results of the Micro-Scale Model MITRAS, J. Atmos. Chem., 44, 113–130, doi:10.1023/A:1022420130032, 2003.

Sievers, U.: Das kleinskalige Strömungsmodell MUKLIMO_3 Teil 1: Theoretische Grundlagen, PC-Basisversion und Validierung, Berichte des Deutschen Wetterdienstes 240, Offenbach am Main, Germany, (German), 2012.

Sievers, U.: Das kleinskalige Strömungsmodell MUKLIMO_3 Teil 2: Thermodynamische Erweiterungen, Berichte des Deutschen Wetterdienstes Entwurf, Offenbach am Main, Germany, (German), 2014.

Skamarock, W. C., Klemp, J. B., Dudhia, J., Gill, D. O., Barker, D., Duda, M. G., yu Huang, X., Wang, W., and Powers, J. G.: A Description of the Advanced Research WRF Version 3, NCAR Tech. Note NCAR/TN-475+STR, 113 pp., NCAR/UCAR, Boulder, 2008.

Tewari, M., Chen, F., W., W., Dudhia, J., LeMone, M. A., Mitchell, K., Gayno, M. Ek, G., Wegiel, J., and H., C. R.: Implementation and verification of the unified NOAH land surface model in the WRF model, pp. 11–15, American Meteorological Society, 20th Conference on Weather Analysis and Forecasting/16th Conference on Numerical Weather Prediction, Seattle, WA, US, presentation, 2004.

United Nations 2014: World Urbanization Prospects: The 2014 Revision, http://esa.un.org/unpd/wup/, last access: 12 December 2016, united Nations, Department of Economic and Social Affairs.

Wicker, L. J. and Skamarock, W. C.: Time-Splitting Methods for Elastic Models Using Forward Time Schemes, Mon. Weather Rev., 130, 2088–2097, doi:10.1175/1520-0493(2002)130<2088:TSMFEM>2.0.CO;2, 2002.

Williamson, J. H.: Low-Storage Runge-Kutta Schemes, J. Comput. Phys., 35, 48–56, doi:10.1016/0021-9991(80)90033-9, 1980.